Journal of Catalysis **190,** 446–459 (2000)
doi:10.1006/jcat.1999.2763, available online at http://www.idealibrary.com on IDEAL®

# Catalytic Reduction of NO by CO over Rhodium Catalysts

## 1. Adsorption and Displacement Characteristics Investigated by *In Situ* FTIR and Transient-MS Techniques

Tarik Chafik,[1] Dimitris I. Kondarides, and Xenophon E. Verykios[2]

*Department of Chemical Engineering, University of Patras, GR-26500 Patras, Greece*

Received September 2, 1999; revised November 16, 1999; accepted November 19, 1999

DEDICATED TO PROFESSOR DR. MANFRED BAERNS ON THE OCCASION OF HIS 65TH BIRTHDAY.

**Adsorption of NO(CO) and displacement by CO(NO) has been investigated at 250°C on Rh catalysts supported on undoped and $W^{6+}$-doped $TiO_2$, employing transient mass spectroscopy and FTIR techniques. It is found that, under the experimental conditions employed, four kinds of nitrogen oxide species may coexist in the adsorbed mode, namely, Rh–$NO^-$(high), Rh–$NO^-$(low), $Rh(NO)_2$, and Rh–$NO^+$, giving rise to IR bands located at 1770, 1660, 1830/1725, and 1908 $cm^{-1}$, respectively. Both negatively charged species readily dissociate on reduced surface sites, yielding nitride, and are mainly responsible for dinitrogen formation in the gas phase. The dinitrosyl species, the formation of which is favored over partially oxidized surfaces, is related to the production of nitrous oxide. The formation of both $N_2$ and $N_2O$ requires the presence of reduced surface sites. In the absence of $Rh^0$, dissociative adsorption of NO stops and Rh–$NO^+$ species dominate the catalyst surface. Doping $TiO_2$ with $W^{6+}$ cations alters the electronic properties of supported Rh crystallites and, concomitantly, the chemisorptive behavior of the catalyst toward NO and CO. In particular, doping results in blue shifts in the stretching frequencies of N–O and C–O bonds contained in Rh–$NO^+$, $Rh(NO)_2$, Rh–CO, and $Rh(CO)_2$ species, indicating a weaker bonding of the adsorbed molecules with the surface. This is also evidenced by the significantly lower amounts of accumulated species, desorbed in TPD experiments. In contrast, the N–O bond of the Rh–$NO^-$ species is weakened by doping, resulting in higher rates of dissociation and, therefore, in higher transient yields of $N_2$ production in the gas phase, compared to the undoped catalyst.** 

### 1. INTRODUCTION

Release of nitrogen oxides from mobile sources has been significantly reduced in recent years with the introduction of three-way catalytic converters (TWCs) for stoichiometrically operated gasoline engines. Current TWCs contain Pt, Pd, and Rh supported on alumina and ceria (1–3), rhodium being a major component due to its high activity and selectivity for catalyzing the reduction of NO by CO. Although currently available TWCs are able to meet rigorous emission standards in gasoline engines, they are not effective for NO reduction under lean-burn applications, such as diesel-fueled vehicles (4, 5). Several explanations have been proposed to account for the decreased activity of Rh to catalyze the NO–CO reaction in the presence of $O_2$, including competition of oxygen and NO for adsorption sites (6), higher reactivity of Rh to catalyze the CO–$O_2$ reaction instead of the NO–CO reaction (7), and deactivation of Rh via the formation of catalytically inactive surface oxide species (8).

Investigation of the formation and reactivity of surface intermediates is crucial for a better understanding of the mechanistic details that govern poisoning effects caused by the high concentration of oxygen contained in the exhaust gas. Combining transient FTIR spectroscopy and mass spectrometry is an effective approach that permits monitoring the evolution of catalyst surface species and the gas phase composition.

CO and NO readily adsorb on reduced Rh surfaces forming a variety of adsorbed species, i.e., linear [$Rh_x$–CO], bridge-bonded [$Rh_2$–CO], and gem-dicarbonyl [$Rh^+(CO)_2$] species (9, 10). Infrared studies of NO chemisorption on Rh catalysts indicate the formation of a cationic [Rh–$NO^+$], a neutral [Rh–NO], and two different anionic [Rh–$NO^-$] species denoted as Rh–$NO^-$ (high) and Rh–$NO^-$(low) (11–27). The difference in the wavenumbers for the latter two species has been attributed to the different extend of electron back-donation from the reduced Rh site to adsorbed NO. It has been suggested that the low wavenumber species, which has been assigned to a bent terminal NO (23; 25 and Refs. therein), is chemisorbed on the surface of large crystallites while the formation of Rh–$NO^-$(high) is favored over highly dispersed Rh (25). The formation of a dinitrosyl [$Rh(NO)_2$] complex has also been reported

[1] Permanent address: Department of Chemistry, Faculty of Science and Technology, University of Tangier, P.O. Box 416, Tangier, Morocco.

[2] To whom correspondence should be addressed. Fax: +30-61-991 527. E-mail: verykios@iceht.forth.gr.



0021-9517/00 $35.00

(15, 16, 21–23), while several nitrate species associated with the support have also been observed (11, 16, 18, 19, 21, 26). Interaction of NO–CO mixtures with Rh catalysts leads to the formation of additional species, including a "fraternal" [Rh(NO)(CO)] structure consisting of a pair of NO and CO molecules adsorbed on the same Rh atom (11, 16, 24), isocyanate (–NCO) (11, 12, 15, 17–21), cyanide (–CN) (12, 14, 17, 19), and carbonate species (11, 16, 18) associated with the metal and/or the support.

Although several IR studies have been carried out to investigate the NO reduction by CO over Rh catalysts, including $Rh/Al_2O_3$ (11, 13–18, 23), $Rh/SiO_2$ (12, 19–22, 25), $Rh/TiO_2$ (22), Rh/MgO (22), and Rh(111) single crystals (27), many uncertainties still exist concerning the nature, type, and reactivity of adsorbed species present on the catalytic surface under reaction conditions.

Work has been carried out in this laboratory to study the effect of catalyst support modification on catalyst performance. It has been shown that the activity of metal crystallites can be significantly enhanced when dispersed on doped semiconductive carriers (28–31). In a recent study in this laboratory, it has been shown that the interaction of NO with $Rh/TiO_2$ and $Rh/TiO_2(W^{6+})$ catalysts proceeds with the dissociation of NO and leads to the formation of $Rh–NO^+$, Rh–NO, and $Rh–NO^-$ species (26). It was argued that $W^{6+}$ doping of titania causes a significant increase in the population of $Rh–NO^-$ species possessing a weaker N–O bond, thus promoting the dissociation of NO to adsorbed N and O atoms (26). To examine the effect of altervalent cation doping of $TiO_2$ on the activity and selectivity of $Rh/TiO_2$ catalysts, a detailed investigation of the $NO/CO/O_2$–Rh system is being carried out in this laboratory, which aims to investigate the mechanistic details of the reduction of NO by CO (or $C_3H_6$), in the presence of oxygen, over Rh dispersed on undoped and doped $TiO_2$.

In the present study, transient-FTIR and -MS experiments have been carried out, to study the interaction of NO and CO with $Rh/TiO_2$ and $Rh/TiO_2(W^{6+})$ catalysts.

## 2. EXPERIMENTAL

### 2.1. Catalyst Preparation and Characterization

The parent titania carrier used was Degussa P25. Doped $TiO_2$ (0.45 at.% $W^{6+}$) was prepared by slurrying appropriate amounts of $TiO_2$ and $WO_3$ in distilled water, followed by evaporation of water at 80°C under continuous stirring, drying of the solid residue at 110°C overnight, and finally, calcining the resulting powder at 900°C for 5 h (26). The $Rh/TiO_2$ and $Rh/TiO_2(W^{6+})$ catalysts were prepared employing the incipient wetness impregnation method using $RhCl_3 \cdot 3H_2O$ (Alfa) as the metal precursor. Weighed amounts of the Rh metal precursor were dissolved in distilled water at 25°C, while an appropriate amount of the carrier was added to the solution under continuous stirring. The suspension was heated at 80°C to evaporate the water and the remaining slurry was dried in an oven at 110°C for 24 h. The dried material was then ground, sieved, and finally treated with $H_2$ at 300°C for 2 h. Metal loading for both catalysts was 0.5% by weight.

Metal dispersion of the undoped catalyst was obtained by extrapolation of the linear part of the $H_2$ chemisorption isotherm at 25°C to zero pressure and was found to be 70% (34 $\mu$mol of $Rh_s/g_{cat.}$) (26). The abnormal $H_2$ chemisorption behavior of $Rh/TiO_2(W^{6+})$ does not allow accurate estimation of Rh dispersion employing this technique. However, TEM analyses revealed that the average crystallite size of the doped catalyst was approximately 20% smaller than that of the undoped and, therefore, Rh dispersion of both catalysts is considered to be approximately the same (26 and Refs. therein).

### 2.2. FTIR Spectroscopy

A Nicolet 740 FTIR spectrometer equipped with a TGS detector and a KBr beam splitter was used in this study (26). Infrared spectra of adsorbed species were obtained with a 32-scan data acquisition at a resolution of 4 $cm^{-1}$ in a controlled gas atmosphere and temperature employing a DRIFT cell (Spectra Tech). During measurements, the external optics were purged with dry air to minimize the level of water vapor and $CO_2$ in the sample chamber. The catalyst, in finely powdered form, was placed into a sample holder and its surface was carefully flattened to increase the intensity of the reflected IR beam.

The cell was directly connected to a flow system, which allowed the application of transient methods (switches in the feed gas composition). All gases used (NO/Ar, CO/Ar, $H_2$, and Ar) were of ultra-high purity. Hydrogen and Ar were further purified employing oxygen traps. In all experiments, the total flow through the DRIFT cell was 35 cc/min.

### 2.3. Transient-MS Experiments

The transient-MS experiments were carried out at 250°C using the apparatus and following the procedure described elsewhere (26). In a typical experiment, 100 mg of the catalyst was placed in a quartz microreactor and reduced at 300°C for 1 h. The sample was then purged with He for 15 min and cooled at 250°C. Transient experiments were then carried out by switching the feed composition to the reactor with the use of chromatographic valves equipped with electronic actuators. At the end of the transient experiments, temperature-programmed desorption (TPD) followed, to quantify the amounts of adsorbed species accumulated on the catalyst. To do this, the feed was switched to He and the temperature was lowered to 200°C. After the sample was purged with He flow for 5 min (total), the catalyst was linearly ($\beta = 30$°C/min) heated to 600°C and TPD spectra were recorded.

Analysis of gases at the effluent of the reactor was done employing an on-line mass spectrometer (Fisons, SPX Elite 300 H) equipped with a fast response inlet capillary/leak diaphragm system. Since the principle peaks of CO and $N_2$ ($m/z = 28$) and $CO_2$ and $N_2O$ ($m/z = 44$) cannot be separated, isotopic $^{15}NO$ was used in all transient-MS experiments reported here. However, for reasons of simplicity, the mass number of isotopic $^{15}NO$ will not be indicated in the following. The concentrations of the gases used in the transient-MS experiments were the same as those used in the corresponding FTIR experiments, but were diluted with He instead of Ar. Furthermore, an amount of Ar (2500 ppm) was also added to the feed. This was done because the Ar response curve represents the flow pattern and the residence time distribution of gaseous reactants flowing through the reactor and the transportation lines, since Ar does not interact with the catalyst. The transient-MS signals at $m/z = 31$ ($^{15}NO$), 30 ($^{15}N_2$), 46 ($^{15}N_2O$), 47 ($^{15}NO_2$), 28 (CO), 44 ($CO_2$), 32 ($O_2$), 18 ($H_2O$), and 40 (Ar) were continuously recorded. Where necessary (e.g., $CO_2$–CO signals), the cracking coefficient determined in separate experiments was also taken into account in the calculations.

Calibration of the mass spectrometer was performed based on self-prepared gas mixtures of accurately known composition. The flow rate in all experiments reported here was 35 ml/min (ambient). It should be mentioned that all experimental conditions (flow rate, mass of catalyst, pretreatment conditions, etc.) were kept the same as the in the corresponding FTIR experiments and, therefore, a direct comparison between the transient-FTIR and -MS results can be made.

## 3. RESULTS

### 3.1. $Rh/TiO_2$ Catalysts

*3.1.1. NO adsorption on $Rh/TiO_2$ and displacement by CO.* The FTIR spectra obtained following exposure of the reduced $Rh/TiO_2$ catalyst to 0.25% NO/Ar at 250°C are shown in Fig. 1, a–c. It is observed that, immediately upon exposure, several bands appear in the spectrum, located at 1912, 1830(sh), 1725, 1660, and 1615 $cm^{-1}$ (Fig. 1, a). After 1 min on stream the bands at 1912, 1830, and 1725 $cm^{-1}$ slightly increase in intensity, the 1660-$cm^{-1}$ band disappears from the spectrum, and a new broad band appears at 1556 $cm^{-1}$ (Fig. 1, b). Prolonged exposure to NO (5 min) does not result in any significant change of the IR bands (Fig. 1, c).

The intense band located at ca. 1912 $cm^{-1}$ may be safely attributed to a positively charged $Rh–NO^+$ species (11–26). The bands located at 1830 (sh) and 1725 $cm^{-1}$ are usually attributed to either neutral (Rh–NO) and negatively charged ($Rh–NO^-$) species, respectively (11–14, 25), or to the $\nu_{sym}$ and $\nu_{asym}$ vibrations of a gem-dinitrosyl complex [$Rh(NO)_2$] (15, 16, 23, 24). As will be shown in the following, the experimental results of the present study show

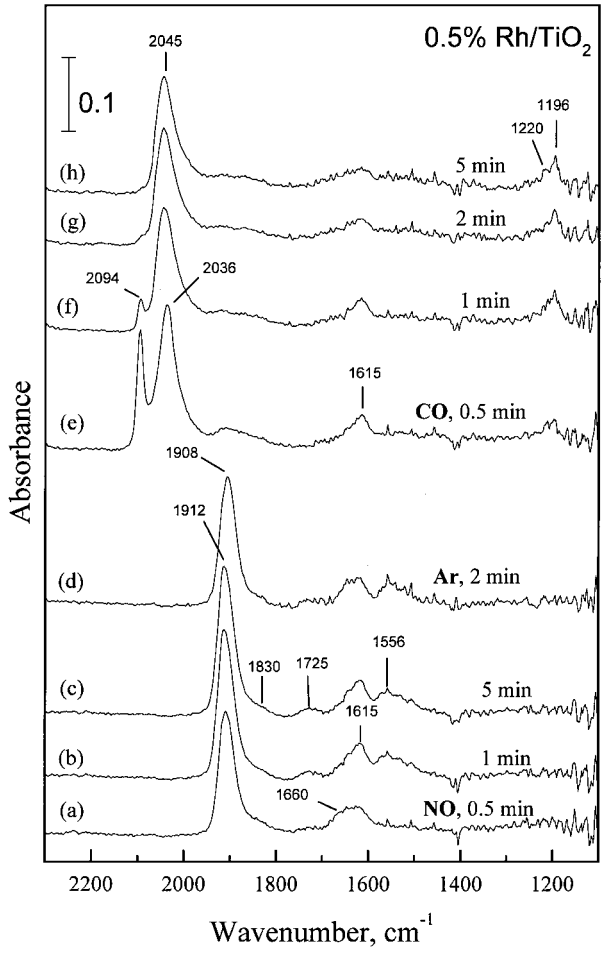


**FIG. 1.** FTIR spectra obtained from 0.5% $Rh/TiO_2$ at 250°C as a function of time-on-stream following the interaction of 0.25% NO/Ar with the reduced catalyst for 0.5, 1, and 5 min (a–c), purging with Ar for 2 min (d), and subsequent switch to 0.5% CO/Ar flow for 0.5, 1, 2, and 5 min (e–h).

that these two bands follow the same trend of appearance/disappearance upon changing experimental conditions without changing their relative intensity, indicating that they originate from the same species. Therefore, the 1830- and 1728-$cm^{-1}$ bands are attributed to the $Rh(NO)_2$ dinitrosyl complex. This assignment was confirmed by isotopic experiments using $^{14}NO$, $^{15}NO$, and $^{14}NO$–$^{15}NO$ mixtures (results will be published separately).

The band at 1660 $cm^{-1}$, which is present during the first minutes-on-stream (Fig. 1, a and b), appears at frequencies much lower than that of gaseous NO (1876 $cm^{-1}$) and may be assigned to a negatively charged nitric oxide species adsorbed on rhodium sites, $Rh–NO^-$(low) (11–13, 18–22, 24, 25). Finally, the bands at 1615 and 1556 $cm^{-1}$ have been previously attributed to nitrate species associated with the support (26 and Refs. therein).

Purging with Ar for 2 min leads to a slight decrease in the intensity of all bands (Fig. 1, d). A subsequent switch to 0.5% CO/Ar results in the progressive disappearance of all bands in the region of 1920–1650 $cm^{-1}$, where the

adsorbed NO species absorb, and in the development of new bands located at 2094 and 2036 $cm^{-1}$, attributable to carbonyl species adsorbed on rhodium (9, 10) (Fig. 1, e). The intensity of the 2094-$cm^{-1}$ band decreases with time of exposure and disappears in less than 2 min on stream. In parallel, the 2036-$cm^{-1}$ peak shifts to higher frequencies and moves to 2045 $cm^{-1}$ after 5 min of exposure (Fig. 1, h). Apart from the bands mentioned above, switching to CO results in the appearance of a band at 1196 $cm^{-1}$, accompanied by a high-frequency shoulder at ca. 1220 $cm^{-1}$, which slightly increases in intensity with time-on-stream (Fig. 1, d–h). The only bands that persist after exposure to CO for 5 min are those located at 2045 and 1196/1220 $cm^{-1}$ as well as broad features at ca. 1885 and 1615 $cm^{-1}$ (Fig. 1, h).

The bands located at 2045 and ca. 1885 $cm^{-1}$ may be safely attributed to linear and bridge-bonded CO on $Rh^0$ sites, respectively (9, 10). The band at 2094 $cm^{-1}$, which is observed only during the first minutes of the transient (Fig. 1, e and f) lies in the region where the asymmetric $\nu$(CO) vibration of the "fraternal" Rh(CO)(NO) species (11, 13–16, 24) and the gem-dicarbonyl $Rh^+(CO)_2$ species are expected to absorb (9, 10). The absence of an accompanying peak in the 1730- to 1750-$cm^{-1}$ region excludes the existence of the fraternal species. The 2094-$cm^{-1}$ band is, therefore, attributed to the $\nu(CO)_{asym}$ vibration of the gem-dicarbonyl $Rh^+(CO)_2$ species whose twin peak at ca. 2032 $cm^{-1}$, indicated by the right-hand side asymmetry of the neighboring peak at 2045 $cm^{-1}$ (attributed to $Rh^0$–CO), is not clearly resolved.

Of special interest are the bands located at 1196/1220 $cm^{-1}$, which appear following interaction of CO with the catalyst (Fig. 1, e–h). These bands appeared in much higher intensity when a 0.25%NO–0.5%CO mixture interacted with the $Rh/TiO_2$ catalysts (results are presented in the second paper of this series (32)). Although bicarbonates bonded on $TiO_2$ may absorb at ca. 1220 $cm^{-1}$ (33), development of the 1220/1196-$cm^{-1}$ bands observed in the present study cannot be attributed to such a species since their appearance/disappearance is not accompanied by similar behavior of bands at ca. 1620 and 1435 $cm^{-1}$ (33). As will be discussed in detail elsewhere (32), the 1220/1196-$cm^{-1}$ bands can be attributed to phenomena associated with the support, i.e., to rupture of Ti–O bonds and surface reduction of $TiO_2$.

Similar experiments have also been conducted employing the transient-MS technique to investigate the transient behavior of reactants and products in the gas phase. The catalyst was first reduced in $H_2$ flow at 300°C for 1 h, purged with He at 300°C for 15 min, and subsequently cooled to 250°C. The reduced catalyst was then exposed to 0.25% NO/He flow for 10 min. The transient responses of NO, $N_2$, $N_2O$, and Ar obtained after the switch, He → 0.25% NO/Ar/He, are presented in Fig. 2A. It is observed that the $N_2$ response appears first, immediately after the switch, and reaches a

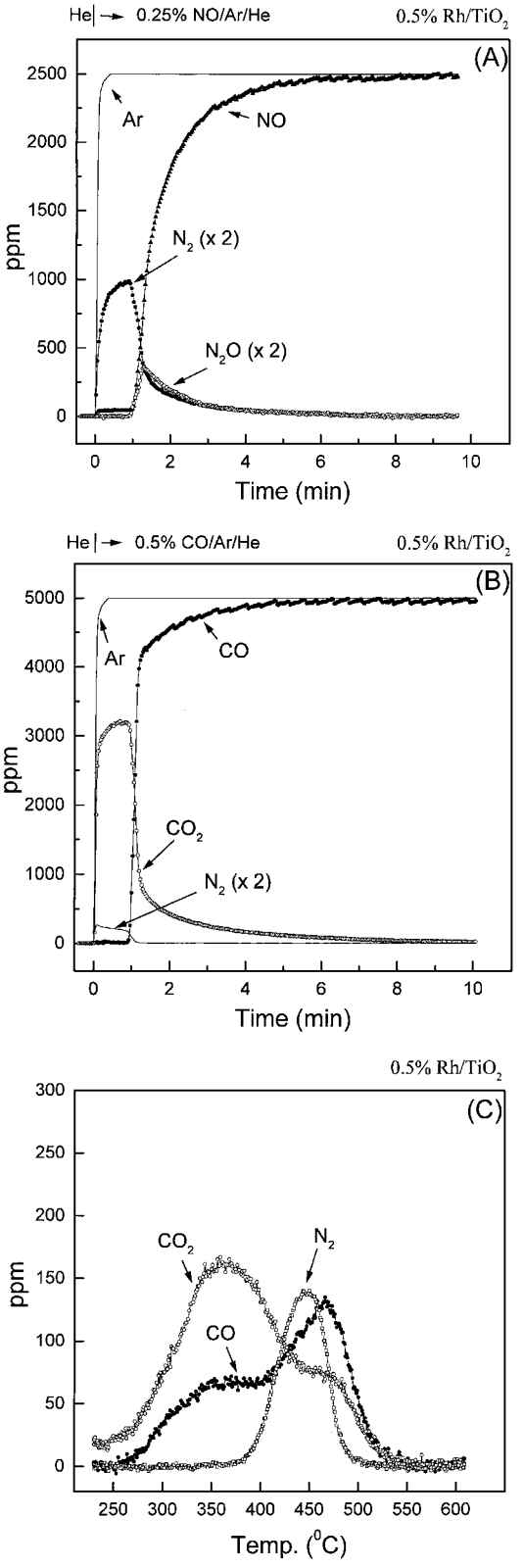


**FIG. 2.** Transient responses of gas phase NO, $N_2$, $N_2O$, CO, $CO_2$, and Ar obtained from 0.5% $Rh/TiO_2$ at 250°C following (A) interaction of the reduced catalyst with 0.25% NO/Ar/He, (B) subsequent treatment with 0.5% CO/Ar/He, and (C) temperature-programmed desorption of accumulated species ($\beta$ = 30°C/min).

plateau. After about 1.0 min on stream, the yield of $N_2$ abruptly decreases and NO starts evolving at the effluent of the reactor. Evolution of NO is accompanied by the formation of $N_2O$, the yield of which peaks at 1.3 min on stream and then gradually decreases. After 10 min on stream, the response of NO reaches its initial value in the feed, indicating that all adsorption and reaction processes have ceased.

Following this treatment, the feed was switched to Ar for 5 min and CO was introduced to the system (Fig. 2B). It is observed that $CO_2$ is produced immediately after the switch, accompanied by the formation of $N_2$. After about 1.0 min on stream, the yields of $CO_2$ and $N_2$ decrease sharply and CO appears at the exit of the reactor.

Results of the subsequent TPD experiments are shown in Fig. 2C, where the responses of desorbed $N_2$, CO, and $CO_2$ are plotted as a function of temperature. $CO_2$ desorbs exhibiting two maxima, an intense one at 360°C and a second one of lower intensity at 470°C. CO desorbs parallel to $CO_2$ and exhibits maxima at the same temperatures. However, the relative peak intensities are reversed; i.e., the high-temperature (HT) peak of CO is more intense than the low-temperature (LT) one. $N_2$ desorbs in a single, symmetric peak with its maximum located at 450°C (Fig. 2C).

The amounts of species formed and consumed in the transient experiments of Figs. 2A and 2B, and the amounts of species desorbed in the subsequent TPD experiment of Fig. 2C, per gram of catalyst, are listed in Table 1. In the same table are also listed similar data obtained from the corresponding experiments presented in the sections which follow.

*3.1.2. CO adsorption on Rh/$TiO_2$ and displacement by NO.* Experimental results obtained following admission of gases with the reverse order over the reduced Rh/$TiO_2$ catalyst at 250°C, i.e., first CO and then NO, are presented in Figs. 3 and 4. The FTIR spectrum obtained after exposure of the reduced catalyst to 0.5% CO/Ar for 5 min is shown in Fig. 3 (a). It is dominated by an intense absorption band located at 2045 $cm^{-1}$ ($Rh^0$–CO), while weaker bands are also observed at 1885 [$(Rh^0)_2CO$], 1620 (carbonates), and 1220/1196 $cm^{-1}$. Purging with Ar for 2 min results in a decrease of the intensity of all bands while the band at 2045 $cm^{-1}$ exhibits a coverage-dependent shift to 2032 $cm^{-1}$ (Fig. 3, b).

Switching the flow from Ar to 0.25% NO/Ar results in an immediate disappearance of the bands due to adsorbed CO species, which are substituted by bands located in the region of 1920–1650 $cm^{-1}$, originating from adsorbed NO species, and bands below 1650 $cm^{-1}$, due to C- and N-containing species associated with the support. The first bands which appear are located at 1908, 1770 (broad), 1660, and 1620 $cm^{-1}$ (Fig. 4, c). The band located at 1770 $cm^{-1}$ is the only one that was not clearly observed following NO adsorption on the reduced catalyst (Fig. 1, a–d). This band may be assigned to a second type of negatively charged NO species, denoted as Rh–$NO^-$(high) (11, 13–15, 18, 22–25).

The 1908-$cm^{-1}$ band develops with time of exposure at a constant frequency and reaches a maximum after 10 min on stream (Fig. 3, c–h). In parallel, the 1770- and 1660-$cm^{-1}$ bands, attributed to the Rh–$NO^-$ species, decrease in intensity and disappear after ca. 2 min on stream (Fig. 3, c–e). It is only then that the bands located at 1725 and ca. 1830 $cm^{-1}$, attributed to the dinitrosyl complex, appear in the spectrum and develop with time-on-stream (Fig. 3, f–h).

As in the case of NO adsorption on the reduced catalyst (Fig. 1, a–c), the band at 1620 $cm^{-1}$ appears immediately

**TABLE 1**

**Amounts ($\mu$mol/$g_{cat.}$) of Species Formed during the Transient-MS and Subsequent TPD Experiments (Sample A, 0.5% Rh/$TiO_2$; Sample B, 0.5% Rh/$TiO_2$($W^{6+}$))**

| Description of experiment | Switch | Sample | Fig. no. | Amounts of species formed/desorbed ($\mu$mol/$g_{cat.}$) | | | | |
|---|---|---|---|---|---|---|---|---|
| | | | | CO | $CO_2$ | NO | $N_2$ | $N_2O$ |
| He → NO → He → CO | He → NO | A | 2A | | | | 11.1 | 4.0 |
| | | B | 6A | | | | 12.7 | 4.1 |
| | He → CO | A | 2B | | 73.8 | 0 | 2.2 | 0 |
| | | B | 6B | | 38.9 | 0 | 2.5 | 0 |
| | TPD | A | 2C | 8.4 | 12.6 | 0 | 4.0 | 0 |
| | | B | 6C | 1.4 | 6.3 | 0 | 3.4 | 0 |
| He → CO → He → NO | He → CO | A | 4A | | 32.3 | | | |
| | | B | 8A | | 4.0 | | | |
| | He → NO | A | 4B | 0 | 13.8 | | 20.7 | 6.8 |
| | | B | 8B | 0 | 6.2 | | 16.1 | 5.6 |
| | TPD | A | 4C | 0 | 5.6 | 2.1 | 11.4 | 0 |
| | | B | 8C | 0 | — | 3.9 | 4.4 | 0 |

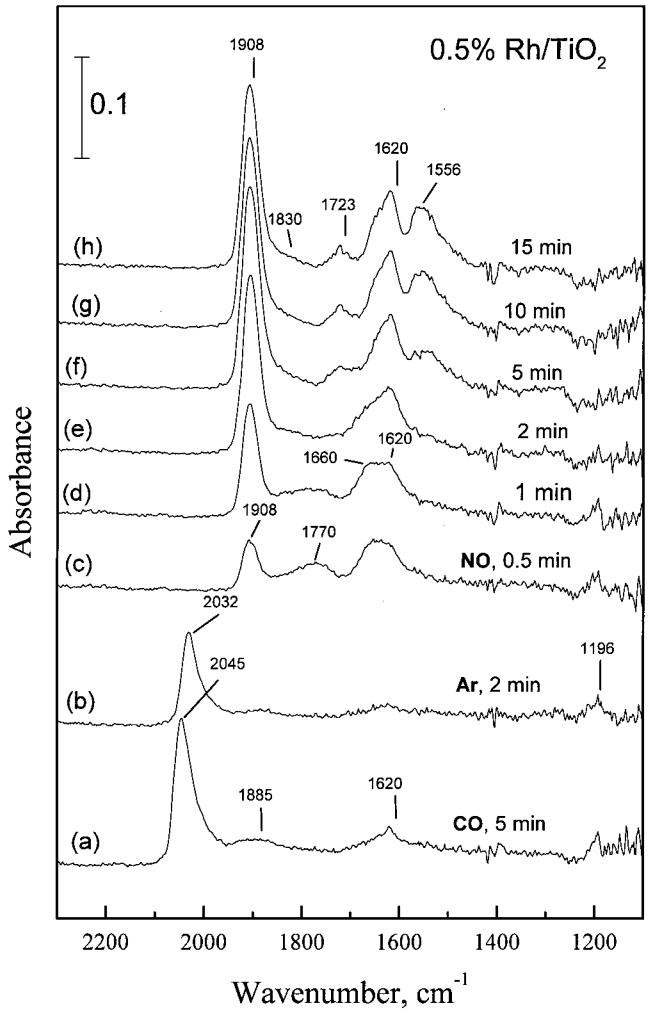


**FIG. 3.** FTIR spectra obtained from 0.5% $Rh/TiO_2$ at 250°C as a function of time-on-stream following interaction of 0.5% CO/Ar with the reduced catalyst for 5 min (a), purging with Ar for 2 min (b), and subsequent switch to 0.25% NO/Ar flow for 0.5, 1, 2, 5, 10, and 15 min (c–h).

upon exposure to NO and gradually increases with time (Fig. 3, c–h). After 2–5 min on stream, the band at 1556 $cm^{-1}$ appears and develops (Fig. 3, e–f). This happens when the bands at 1770 and 1660 $cm^{-1}$ disappear and the bands at 1830 and 1725 $cm^{-1}$ start to develop. Finally, the band located at 1220/1196 $cm^{-1}$ decreases with time-on-stream upon exposure to NO flow and disappears after ca. 2 min (Fig. 3, c–e).

The corresponding transient-MS experiments are presented in Figs. 4A–4C. Interaction of the reduced catalyst with 0.5% CO/He at 250°C results in the formation of $CO_2$, which exhibits a sharp peak a few seconds after the introduction of CO, and then gradually decreases with time-on-stream (Fig. 4A). The formation of $CO_2$ could be due to dissociation of CO and/or reaction of CO with oxygen originating from the support. The latter could explain the appearance of the 1220/1196-$cm^{-1}$ band (Fig. 3), as discussed

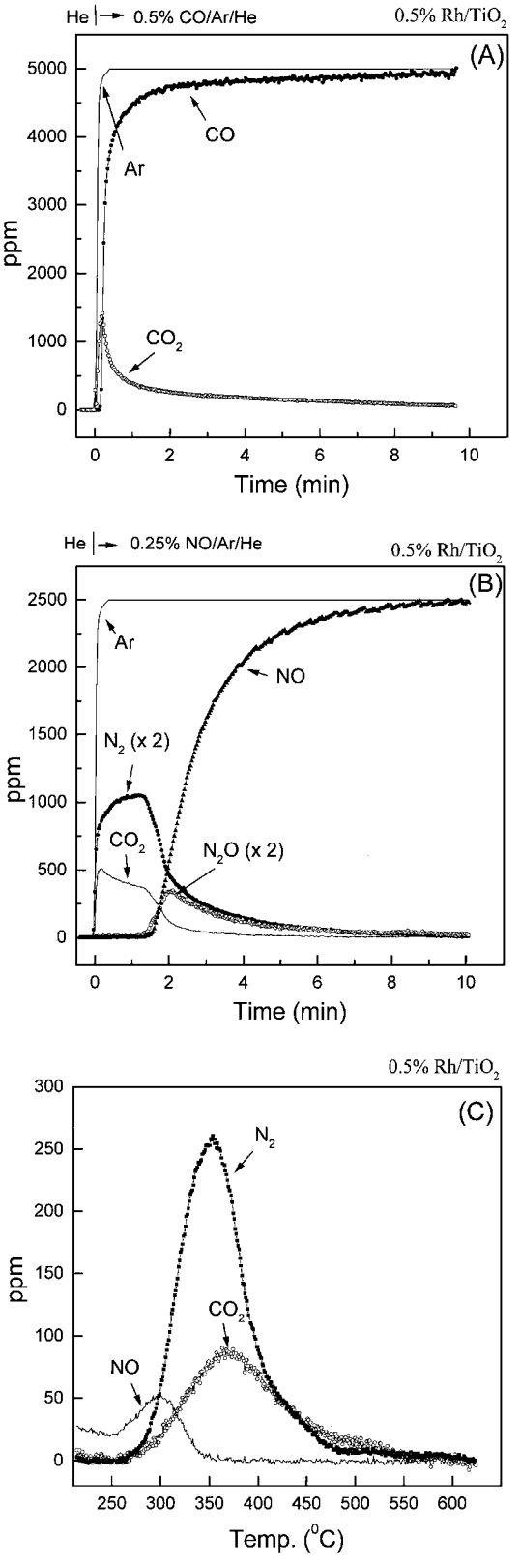


**FIG. 4.** Transient responses of gas phase NO, $N_2$, $N_2O$, CO, $CO_2$, and Ar obtained from 0.5% $Rh/TiO_2$ at 250°C following (A) interaction of the reduced catalyst with 0.5% CO/Ar/He, (B) subsequent treatment with 0.25% NO/Ar/He, and (C) temperature-programmed desorption of accumulated species ($\beta = 30$°C/min).

above. The lag between the responses of Ar and CO is due to CO adsorption and reaction to $CO_2$, which take place upon interaction of the reduced catalyst with CO.

The system was then purged with Ar and 0.25% NO/He was introduced to the reactor at 250°C (Fig. 4B). It is observed that during the first 1.5 min after the switch, only $N_2$ and $CO_2$ appear at the exit of the reactor. Then, NO starts evolving and the yields of $N_2$ and $CO_2$ start to decrease. As soon as NO appears, the formation of $N_2O$ takes place, the yield of which peaks at 2.0 min on stream and then gradually drops. After 10 min on stream, the response of NO reaches its initial value, indicating that all adsorption and reaction processes have ceased (Fig. 4B).

The TPD curves of the species accumulated on the catalyst surface following the treatment described above are presented in Fig. 4C. A peak of NO appears first with its maximum located at ca. 300°C. $N_2$ and $CO_2$ start evolving simultaneously and exhibit single peaks with their maxima locating at 350 and 370°C, respectively.

### 3.2. *Rh/TiO$_2$(W$^{6+}$) Catalysts*

*3.2.1. NO adsorption on Rh/TiO$_2$(W$^{6+}$) and displacement by CO.* The FTIR bands obtained following interaction of 0.25% NO/Ar with the reduced Rh/TiO$_2$(W$^{6+}$) catalyst (Fig. 5, a–c) are similar to those observed over the undoped Rh/TiO$_2$ catalyst, but shifted to higher frequencies, and may also be attributed to Rh–NO$^+$ (1920 cm$^{-1}$), Rh(NO)$_2$ (1880 and 1750 cm$^{-1}$), Rh–NO$^-$(low) (ca. 1660 cm$^{-1}$), and nitrate species associated with the support (bands below 1650 cm$^{-1}$). The intensity of all bands slightly decreases with time-on-stream, while the band at ca. 1660 cm$^{-1}$ disappears after 5 min (Fig. 5, c).

Purging with Ar and subsequent interaction of the NO-precovered surface with 0.5% CO/Ar results in the progressive decrease of the bands at 1920, 1880, and 1750 cm$^{-1}$, and the development of weak bands above 2000 cm$^{-1}$, attributable to carbonyl species on oxidized rhodium sites (9, 10) (Fig. 5, g). When the former bands disappear from the spectrum, after ca. 5 min on stream, the spectrum is dominated by the twin bands at 2106 and 2044 cm$^{-1}$, attributed to gem-dicarbonyl and monocarbonyl species (Fig. 5, h). Prolonged exposure to CO results in the reduction of rhodium, as indicated by the dominance of bands at 2050 and ca. 1900 cm$^{-1}$, due to linear and bridge-bonded CO on Rh$^0$ sites. These bands are accompanied by bands below 1650 cm$^{-1}$ due to carbonate species (Fig. 5, j).

The corresponding transient-MS results are presented in Fig. 6. The transient responses of NO, $N_2$, and $N_2O$ obtained after the switch He → 0.25% NO/Ar/He, shown in Fig. 6A, are qualitatively similar to those obtained over the undoped catalyst (Fig. 2A). However, the amounts of NO consumed and $N_2$ and $N_2O$ formed are somewhat larger (Table 1).

Interaction of the adsorbed species with CO at 250°C again results in the production of large amounts of $CO_2$ and small amounts of $N_2$ (Fig. 6B). In the subsequent TPD experiments, small amounts (compared with the undoped catalyst) of $CO_2$ and $N_2$ are desorbed, exhibiting maxima at ca. 360 and 420°C, respectively (Fig. 6C). Desorption of small amounts of CO is also observed in the region of 300–470°C (Fig. 6C).

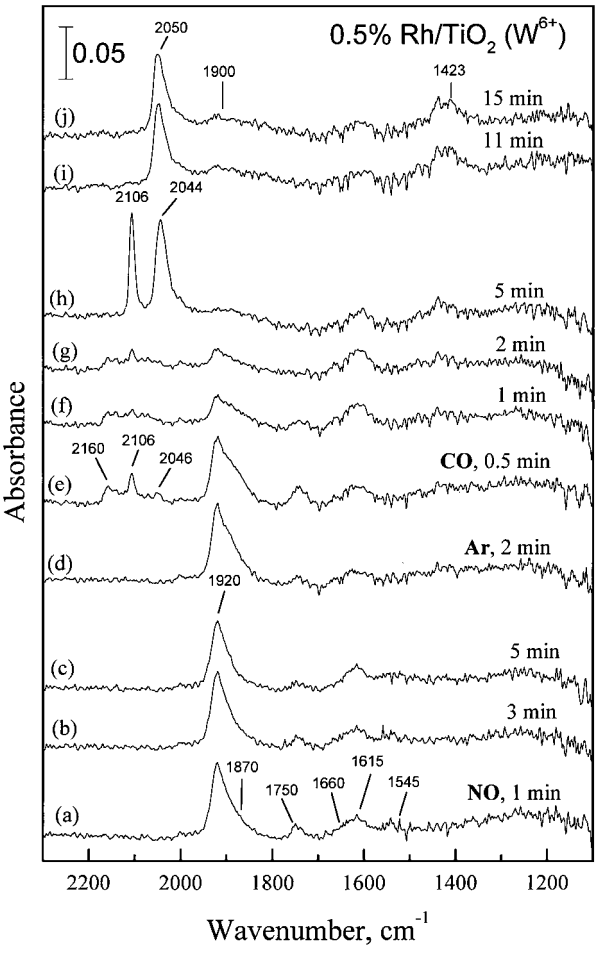


**FIG. 5.** FTIR spectra obtained from 0.5% Rh/TiO$_2$(W$^{6+}$) at 250°C as a function of time-on-stream following interaction of 0.25% NO/Ar with the reduced catalyst for 1, 3, and 5 min (a–c), purging with Ar for 2 min (d), and subsequent switch to 0.5% CO/Ar flow for 0.5, 1, 2, 5, 11, and 15 min (e–j).

*3.2.2. CO adsorption on Rh/TiO$_2$(W$^{6+}$) and displacement by NO.* The spectrum obtained following interaction of CO with reduced Rh/TiO$_2$(W$^{6+}$) is characterized by bands due to linear and bridge-bonded CO on Rh$^0$ (2050, 1900 cm$^{-1}$) and carbonates at 1615 and 1430 cm$^{-1}$ (Fig. 7, a). The fact that IR bands below 1650 cm$^{-1}$ are, in general, of less intensity over the doped catalyst is due to the larger BET surface area of $TiO_2$ (anatase) as compared to that of W$^{6+}$-doped $TiO_2$ (calcined at 900°C).

Switching the flow from Ar to 0.25% NO/Ar leads to the immediate disappearance of the carbonyl bands, which

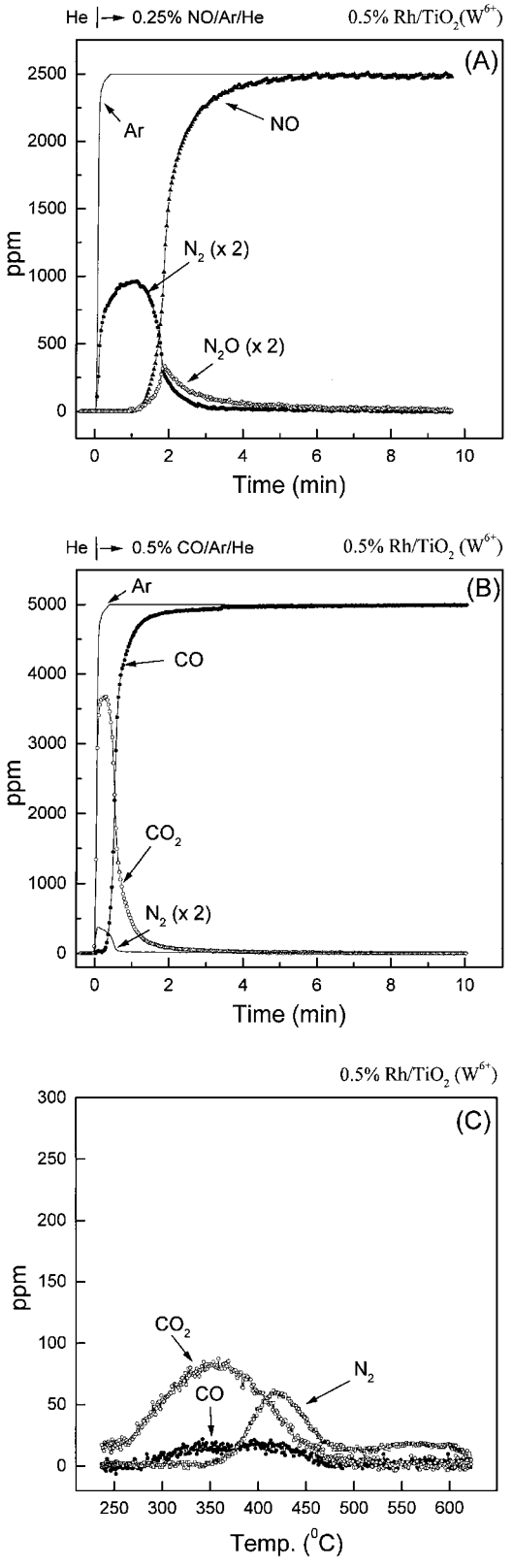


**FIG. 6.** Transient responses of gas phase NO, $N_2$, $N_2O$, CO, $CO_2$, and Ar obtained from 0.5% $Rh/TiO_2(W^{6+})$ at 250°C following (A) interaction of the reduced catalyst with 0.25% NO/Ar/He, (B) subsequent treatment with 0.5% CO/Ar/He, and (C) temperature-programmed desorption of accumulated species ($\beta = 30$°C/min).

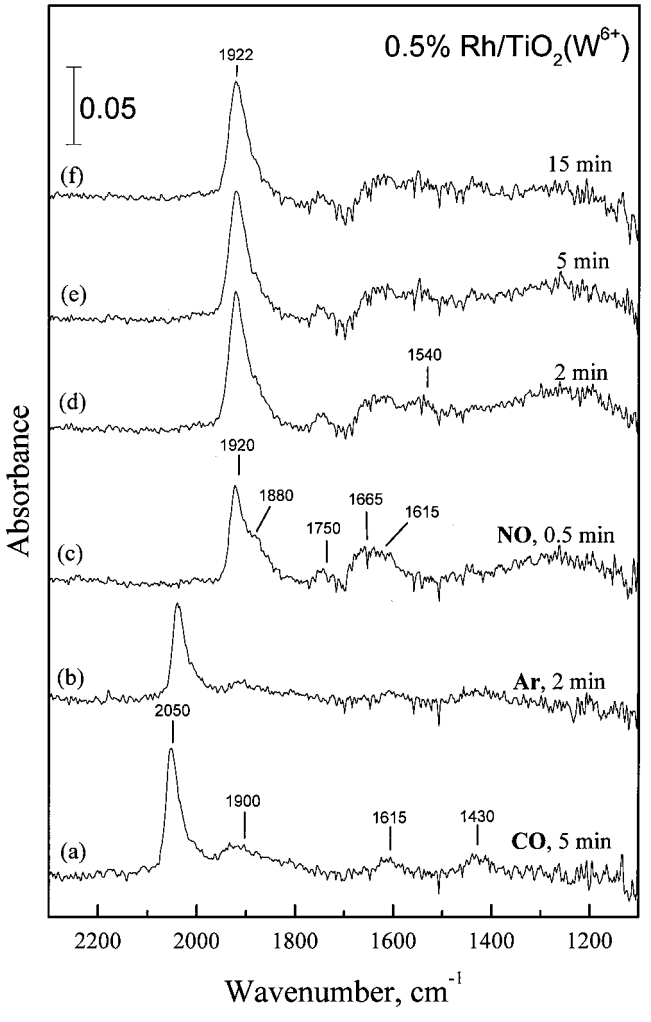


**FIG. 7.** FTIR spectra obtained from 0.5% $Rh/TiO_2(W^{6+})$ at 250°C as a function of time-on-stream following interaction of 0.5% CO/Ar with the reduced catalyst for 5 min (a), purging with Ar for 2 min (b), and subsequent switch to 0.25% NO/Ar flow for 0.5, 2, 5, and 15 min (c–f).

are displaced by bands in the $\nu$(N–O) stretching region (Fig. 7, c). The HF band of the dinitrosyl species, located at 1880 $cm^{-1}$, is more clearly resolved now. Increasing the time of exposure results in the full development of the 1920-$cm^{-1}$ band and the decrease of the intensity of the 1660-$cm^{-1}$ band (Fig. 7, c–f).

Results of the corresponding transient-MS experiments are presented in Fig. 8. Interestingly, interaction of 0.5% CO/Ar with the reduced catalyst (Fig. 8A) results in the production of very small amounts of $CO_2$, compared to the undoped catalyst (Fig. 4A, Table 1). The responses of reactants and products obtained following interaction of the CO-precovered surface with 0.25% NO/Ar are qualitatively similar to those obtained from the undoped catalyst (Fig. 8B). In the subsequent TPD experiment, only NO and $N_2$ were desorbed from the surface, exhibiting maxima at ca. 320 and 370°C (Fig. 8C). No detectable amounts of CO and $CO_2$ were desorbed.

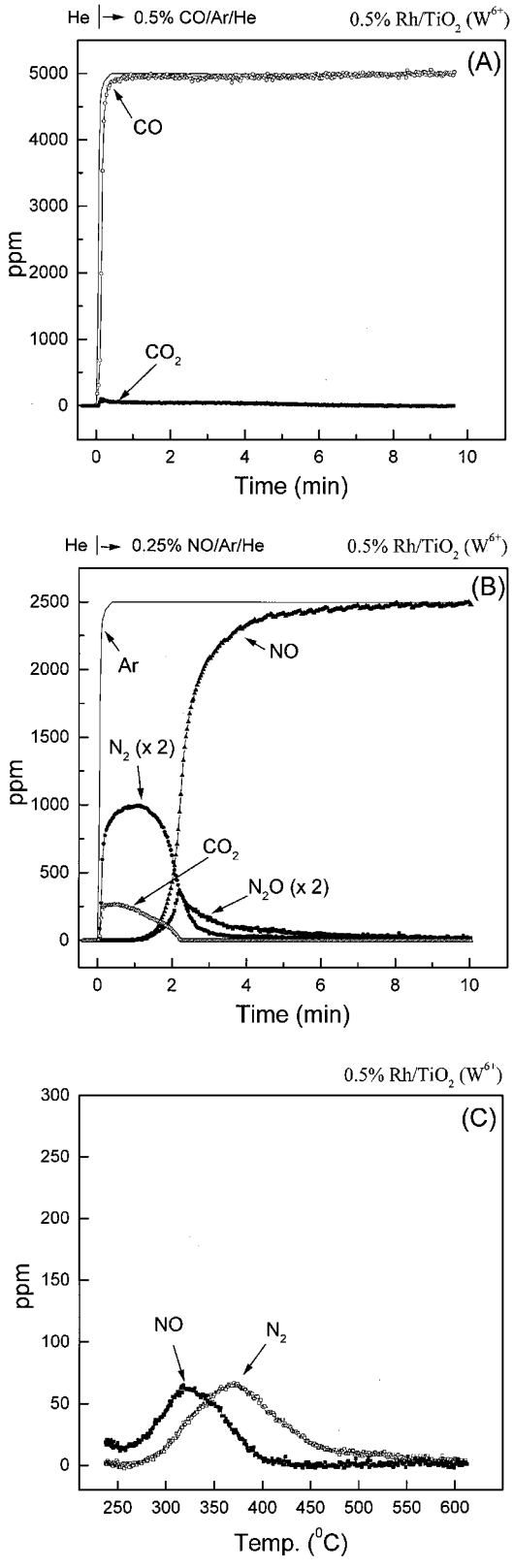


**FIG. 8.** Transient responses of gas phase NO, $N_2$, $N_2O$, CO, $CO_2$, and Ar obtained from 0.5% $Rh/TiO_2(W^{6+})$ at 250°C following (A) interaction of the reduced catalyst with 0.5% CO/Ar/He, (B) subsequent treatment with 0.25% NO/Ar/He, and (C) temperature-programmed desorption of accumulated species ($\beta = 30$°C/min).

## 4. DISCUSSION

### *4.1. Interaction of NO with Reduced $Rh/TiO_2$ and Displacement by CO*

Interaction of 0.25% NO with $H_2$-reduced $Rh/TiO_2$ surfaces at 250°C results in the appearance of bands due to $Rh–NO^+$, $Rh(NO)_2$, and $Rh–NO^-$ (low) species and bands due to N-containing species associated with the support (Fig. 1, a–c). The band due to $Rh–NO^-$ (high), which is clearly observed in the corresponding experiment over the CO-precovered surface (Fig. 3, c–h), is not discernible here. However, its presence in the initial steps of the experiment cannot be excluded. $Rh–NO^-$ species are present during the initial steps of NO adsorption but decrease in population with time of exposure before disappearing from the spectra after ca. 1 min on stream (Fig, 1, a–c). The low stretching frequency of $Rh–NO^-$ is indicative of the weakening of the N–O bond and the strengthening of the Rh–N bond, which results in the higher propensity of this species to dissociate over reduced Rh surfaces to produce nitride and adsorbed oxygen atoms:

$$Rh^0–NO^- + Rh^0 \rightarrow Rh–N + Rh–O. \quad [1]$$

As NO dissociates on reduced Rh sites, oxygen atoms accumulate on the surface and assert an electron-withdrawal effect on Rh which, in turn, is passed onto the molecularly adsorbed nitrogen oxide molecules which become slightly positively charged (14). Formation of $Rh–NO^+$ may also arise from the adsorption of NO molecules on oxidized rhodium sites (15):

$$Rh–O + NO_{(g)} \rightarrow Rh(O)(NO). \quad [2]$$

In Eq. [2], Rh(O)(NO) does not refer to coadsorbed O and NO species but to adsorption of NO on an oxidized rhodium site.

It is very interesting to note that the $Rh–NO^+$ band at 1912 $cm^{-1}$ fully develops only when the bands due to $Rh–NO^-$ species disappear from the spectra (Fig. 1, a–c), i.e., when there are no reduced Rh sites left for the dissociation of NO. NO adsorption then ceases due to accumulation of oxygen atoms (Eq. [1]).

Concerning the formation of the $Rh(NO)_2$ species (1830 and 1725 $cm^{-1}$), it is believed that it probably exists at individual Rh atom sites or edge sites with cationic character generated through interactions between metal atoms and the support, by analogy to the formation of the gem-dicarbonyl species (15), i.e.,

$$Rh^0–NO + OH^- + NO \leftrightarrow Rh^+(NO)_2 + O^{2-} + \tfrac{1}{2}H_2. \quad [3]$$

As observed in Fig. 1, a–c, and, especially, in Fig. 3, c–h, the 1830- and 1728-$cm^{-1}$ bands do not appear immediately upon exposure of the catalyst to NO but develop only

when the bands at 1770 and 1660 $cm^{-1}$ ($Rh–NO^-$) disappear from the spectra. This indicates that the formation of the dinitrosyl species is associated with the existence of oxidized rhodium sites. It is, therefore, possible that the formation of the dinitrosyl complex may also arise from interaction of positively charged $Rh–NO^+$ with gaseous nitrogen oxide:

$$Rh–NO^+ + NO_{(g)} \rightarrow Rh(NO)_2. \quad [4]$$

This is consistent with the results of Liang *et al.* (23) who suggested that some degree of reversibility exists between the $Rh(NO)_2$ and $Rh–NO^+$ species. Prolonged exposure to NO does not result in further increase of the 1830- and 1725-$cm^{-1}$ band intensities, which reach a plateau when the 1912-$cm^{-1}$ band reaches its maximum intensity. The population of $Rh(NO)_2$ does not further increase when oxygen atoms (produced by Eq. [1]) completely "poison" the surface. Hyde *et al.* (15) proposed that oxygen adatoms produced during the formation of $Rh–NO^+$ block the formation of $Rh(NO)_2$.

Concerning the behavior of the bands at 1615 and 1556 $cm^{-1}$, attributed to N-containing species associated with the support, the former appears in the spectra immediately following interaction of the catalyst with NO, while the latter develops only when the negatively charged $Rh–NO^-$ species are removed from the surface and the band due to $Rh–NO^+$ fully develops (Fig. 1, a–c). This indicates that the species absorbing at ca. 1556 $cm^{-1}$ is probably formed by the reaction of $Rh–NO^+$ with adsorbed atomic oxygen (18):

$$Rh–NO^+ + 2O_{ad} \leftrightarrow (NO_3)_{ad} + Rh^+. \quad [5]$$

FTIR results discussed above may be correlated with the corresponding results obtained from the transient-MS experiments: Interaction of NO with the $H_2$-reduced catalyst at 250°C results, initially, in the production of only $N_2$ in the gas phase, while the formation of $N_2O$ takes place when the yield of $N_2$ starts to decrease and NO appears at the effluent of the reactor (Fig. 2A). Comparison of the FTIR spectra of Fig. 1, a–c, with the transient-MS results of Fig. 2A, shows that formation of dinitrogen coincides with the presence of $Rh–NO^-$ species on the surface. On the other hand, the formation of $N_2O$ and the appearance of gas phase NO at the effluent of the reactor are related to the appearance and full development of the $Rh(NO)_2$ and $Rh–NO^+$ species on the catalyst surface. These observations are more pronounced in the corresponding FTIR (Fig. 3, c–h) and transient-MS (Fig. 4B) experiments obtained over the CO-precovered surface, discussed in the following paragraphs.

The dynamic behavior of the responses of reactants and products may be correlated with the type and population of surface species as follows: Interaction of NO with the catalyst initially leads to the formation of $Rh–NO^+$ and $Rh–NO^-$ species (Fig. 1, a–c). Adsorbed nitrogen atoms may then combine and/or react with adsorbed NO species to yield dinitrogen in the gas phase, as observed in Fig. 2A:

$$Rh–N + Rh–N \rightarrow N_{2(g)} + 2Rh^0; \quad [6]$$

$$Rh–NO^- + Rh–N \rightarrow N_2 + Rh–O + Rh^0. \quad [7]$$

However, dissociative adsorption of NO also results in the accumulation of oxygen atoms on the catalyst (Eq. [1]), which cannot be removed from the surface under the present conditions. This results in progressive oxidation of rhodium sites, in a decrease of the population of $Rh–NO^-$ on the surface, and concomitantly, in a progressive decrease of the yield of $N_2$. When reduced rhodium sites become less available, NO starts appearing at the exit of the reactor (Fig. 2A). In parallel, the population of $Rh–NO^-$ species gradually decreases and the population of $Rh–NO^+$ increases with time-on-stream (Fig. 2, a–c). The dominance of $Rh–NO^+$ species on the catalyst surface indicates that all adsorption processes have ceased. When this happens, the NO concentration at the exit of the reactor reaches that of the feed (Fig. 2A).

Of special interest is the formation of $N_2O$, which takes place only when NO starts evolving at the exit of the reactor and ceases when NO concentration reaches that of the feed. The formation of $N_2O$ may be correlated with the appearance of the dinitrosyl complex on the catalyst surface. Both the formation of $Rh(NO)_2$ on the surface and $N_2O$ in the gas phase are observed over surfaces which are partly but not completely oxidized. It should be noted that the surface state of the catalyst during the transient is changing from that of a reduced one ($H_2$ and CO pretreatment) to an oxidized one (NO adsorption), and vice versa, due to the inability of the system to remove accumulated oxygen atoms from the surface. When the catalyst is "poisoned" by adsorbed oxygen and the $Rh–NO^+$ species dominates, the formation of $N_2O$ stops (e.g., Figs. 2A and 4B) and the population of gem-dinitrosyl reaches a plateau (Figs. 1, c; 3, h). It is, therefore, possible that the formation of $N_2O$ in the present experiments requires the presence of both the gem-dinitrosyl species and neighboring reduced rhodium sites, as was proposed by Anderson *et al.* (16):

$$Rh(NO)_2 + Rh^0 + NO \rightarrow Rh–NO^+ + Rh–O^- + N_2O_{(g)}. \quad [8]$$

Reaction (8) accounts for the formation of $N_2O$ in the gas phase which stops because, as in the case of NO dissociation discussed above, the reactive sites are simultaneously poisoned by an oxygen adatom, which prevents further reaction. This is in accordance with the results of Hyde *et al.* (15) and the molecular orbital calculations of Casewit and Rappe (34) who proposed that the formation of the dinitrosyl complex is an intermediate step in the formation of $N_2O$ from NO on Fe(II) catalysts. The formation of $N_2O$ stops when there are no free $Rh^0$ sites left, neighboring to the dinitrosyl species. It should be noted that, under the

present experimental conditions, the formation of nitrous oxide via the reaction

$$Rh^0\text{–}NO^- + Rh^0\text{–}N \rightarrow 2Rh^0 + N_2O \quad [9]$$

proposed by others (e.g., (20)) may be excluded, since only $N_2$, but not $N_2O$, is formed during the initial steps of the transients, although both $Rh^0$–N the Rh–$NO^-$ species are present on the surface.

FTIR and transient-MS experiments probing interaction of CO with NO-precovered surfaces at 250°C (Figs. 1, e–h, and 2B) show that exposure to CO leads to a rapid displacement of the bands in the 1920- to 1650-$cm^{-1}$ region, which are substituted by bands in the $\nu$(C–O) region (Fig. 1, e–h). The appearance of gem-dicarbonyl bands at 2094 and ca. 2032 $cm^{-1}$ (not resolved) immediately after switching to CO gives additional evidence that rhodium becomes partially oxidized following NO adsorption and confirms the role of NO in promoting oxidative disruption of Rh crystallites (13). Increasing the time of exposure results in the reductive agglomeration of Rh crystallites, which is expected to take place at 250°C, and to progressive reduction of the catalyst by CO as indicated by the dominance of $Rh^0$–CO (2045 $cm^{-1}$) after more than 2 min on stream.

These phenomena are also reflected in the gas phase, where $CO_2$ production is observed during the first minutes of the transient (Fig. 2B):

$$Rh\text{–}O + CO_{(g)} \rightarrow CO_{2(g)} + Rh^0. \quad [10]$$

When the catalyst surface is depleted of adsorbed atomic oxygen, the yield of $CO_2$ decreases with time-on-stream and gradually drops to zero, while the concentration of CO progressively reaches that of the feed (Fig. 1B). The appearance of the band at 1196 $cm^{-1}$ (Fig. 1, e–h) and the formation of small amounts of $CO_2$ for several minutes following exposure to CO (Fig. 2B) indicate that incoming CO also interacts with oxygen atoms originating from the carrier, thus reducing titania,

$$TiO_2 + xCO \rightarrow TiO_{2-x} + xCO_2. \quad [11]$$

Apart from $CO_2$, small amounts of $N_2$ are also produced during the first minute of the transient (Fig. 1B). Dinitrogen may be formed either by recombination of Rh–N species (Eq. [2]), which are removed from the surface and are replaced by CO molecules, and/or by reaction of incoming or adsorbed CO with adsorbed NO:

$$Rh\text{–}NO + CO \rightarrow Rh\text{–}N + CO_{2(g)}. \quad [12]$$

The fact that production of $N_2$ is observed in the gas phase (Fig. 2B) under conditions where no adsorbed NO is detected (Fig. 1, e,f) is due to the existence of Rh–N species on the catalyst surface which, although present, cannot be detected under the present experimental conditions. However, treatment of the NO-precovered surface with CO/He for 12 min (Fig. 2B) is not adequate to remove all nitrogen-containing species from the surface. This is clearly shown in the subsequent TPD experiment, where a significant amount of $N_2$ (4.0 $\mu$mol/$g_{cat}$) is observed to desorb at ca. 450°C (Fig. 2C, Table 1). In the same experiment, amounts of CO and $CO_2$ are also desorbed from the surface giving peaks at 360 and 370°C, respectively (Fig. 2C). Concerning the origin of the desorbing $N_2$, the following arguments can be made: Since in the corresponding FTIR experiments no molecularly adsorbed NO was observed on the catalyst surface following treatment with CO at 250°C (Fig. 1, h), $N_2$ observed in the TPD spectra of Fig. 2C may either originate from Rh–N species that survived on the surface and/or from the decomposition of N-containing species associated with the support. As discussed in a previous paragraph, the formation of nitrates may be represented by Eq. [5]. Heating the sample during the TPD experiment may result in a shift of Eq. [5] to the left, i.e., to the decomposition of $(NO_3)_{ad}$ and in the formation of Rh–NO and Rh–O. The former species may then react with adsorbed CO to form Rh–N (and then dinitrogen in the gas phase), while the latter reacts with adsorbed CO to yield $CO_2$. The TPD peaks of CO and $CO_2$ observed in Fig. 2C are partly formed in the way discussed above and partly through the standard processes of CO desorption from Rh surfaces.

### *4.2. Interaction of CO with Reduced Rh/$TiO_2$ and Displacement by NO*

Results of the FTIR experiments conducted by first introducing CO and then NO over the Rh/$TiO_2$ catalyst at 250°C are shown in Fig. 3, and the corresponding transient-MS experiments are presented in Fig. 4. Exposure of the $H_2$-reduced catalyst to CO leads to the formation of linear and bridged CO on $Rh^0$ sites, as well as to the development of the 1220/1196-$cm^{-1}$ band associated with the reduction of the support (Fig. 3, a). Concerning the gas phase, the formation of $CO_2$ is observed (Fig. 4A), originating from dissociation of CO and/or reaction of CO with oxygen originating from the support. The latter possibility explains the appearance of the 1220/1196-$cm^{-1}$ band (Fig. 3), as discussed above. Interaction of the CO-precovered surface with NO results in the development of bands due to Rh–$NO^+$, $Rh(NO)_2$, Rh–$NO^-$, and $(NO_3)_a$ species (Fig. 3, c–h). The formation and disappearance of these species on the surface occurs in a way similar to that observed over the $H_2$-reduced catalyst (Fig. 1, a–c), but all processes are slower and, therefore, more clearly distinguished.

Bands due to Rh–$NO^-$(high) and Rh–$NO^-$(low) species are present in the FTIR spectra during the first 2 min of exposure to NO (Fig. 3, c–e). During this time period, only $CO_2$ and $N_2$ appear at the exit of the reactor in the corresponding transient-MS experiments (Fig. 4B). Interestingly,

no gas phase CO is observed, implying that adsorbed CO species are not directly replaced by incoming NO molecules but are transformed to C-containing species associated with the support which then react with surface oxygen species to yield $CO_2$. It is clear that only when the Rh–$NO^-$ bands disappear from the spectra, after ca. 2 min on stream, the bands due to dinitrosyl species appear and the band of positively charged NO fully develops (Fig. 3, f–h). When this happens, the responses of $N_2$ and $CO_2$ sharply decrease and NO appears at the exit of the reactor, accompanied by $N_2O$ formation (Fig 4B).

Comparison of the FTIR and transient-MS results obtained following the interaction of NO with $H_2$-reduced (Figs. 1, a–c, and 2B) and CO-precovered (Figs. 3, c–h, and 4B) surfaces clearly shows that different times of exposure to NO are required for the complete disappearance of Rh–$NO^-$ and the full development of Rh–$NO^+$ species over differently pretreated catalyst surfaces (about 1 min for the $H_2$-reduced and 2 min for the CO-precovered surface). These time periods coincide with the time-on-stream elapsed before NO starts appearing at the effluent of the reactor in the transient-MS experiments. In addition, it is observed that the amount of $N_2O$ formed over $H_2$-reduced and CO-precovered surfaces is practically the same, i.e., 5.1 and 7.1 $\mu$mol/$g_{cat.}$, respectively. However, the corresponding amounts of $N_2$ produced are 11.1 and 20.7 $\mu$mol/$g_{cat.}$ (Table 1). This behavior strongly indicates that, in the CO-precovered surface, an oxygen-atom scavenger is present on the surface, which removes oxygen and prevents oxidation of active sites. Since bands due to adsorbed CO disappear immediately after the switch to NO (Fig. 3), it is the C-containing species present on the catalyst that play that role. However, results of the present study indicate that part of oxygen scavenging is due to $TiO_{2-x}$ species (produced through Eq. [11]) in the vicinity of Rh crystallites: There is a correlation between the time required for the oxidation of the catalyst surface and the presence and intensity of the bands at 1220/1196 $cm^{-1}$. Over the $H_2$-reduced catalyst these bands are absent and oxidation of the Rh active sites is rapid (Fig. 3, a–c). However, over the CO-precovered catalyst, the 1220/1196-$cm^{-1}$ bands are present and gradually decrease in intensity with time of exposure to NO, before disappearing after 2 min on stream (Fig. 3, c–f). This decrease is accompanied by the disappearance of the Rh–$NO^-$ bands and the full development of the Rh–$NO^+$ band discussed above. Reduced titania may then act as an oxygen-atom scavenger, thus leading to the regeneration of the active rhodium sites:

$$TiO_{2-x} + x\,Rh\text{–}O \rightarrow TiO_2 + x\,Rh^0. \qquad [13]$$

When the initial state of the support is restored, as indicated by the disappearance of the 1220/1196-$cm^{-1}$ bands, scavenging of adsorbed oxygen atoms stops, atomic oxygen accumulates on the catalyst surface, and all NO adsorption processes cease (Figs. 3, 4, and 9). This observation gives additional evidence that the 1220/1196-$cm^{-1}$ bands are related to the reduction of $TiO_2$ in the vicinity of the interface with Rh crystallites and the formation of $TiO_{2-x}$. This subject will be discussed in more detail elsewhere (32). The increased amount of $N_2$ produced and the longer time period required for the appearance of NO in the gas phase, compared to that over the $H_2$-reduced catalyst (Fig. 1A) is, therefore, attributed to the presence of more reducible material (i.e., adsorbed CO and $TiO_{2-x}$) on the catalyst in the experiment in Fig. 2B.

In the subsequent TPD spectra (Fig. 4C), it is observed that not only NO and $N_2O$ but also $CO_2$ is desorbed from the catalyst surface. Since no adsorbed CO is observed in the corresponding FTIR experiments following the interaction of NO with CO-precovered surfaces (Fig. 3, h), it is assumed that $CO_2$ formation is associated with decomposition of carbonate-type species.

Comparison of the TPD spectra presented in Fig. 4C with those of Fig. 2C shows a significant difference in the temperature of maximum intensity of the TPD peaks of $N_2$ (350 and 440°C, respectively). Several studies on single crystals and supported Rh catalysts show that nitrogen evolution of adsorbed NO shows, in general, two peaks: one centered at 180–210°C (denoted as $\beta_1$) and a second at ca. 280–460°C (denoted as $\beta_2$), which are attributed, respectively, to the following processes (21, 41–43),

$$NO_{(a)} + N_{(a)} \rightarrow N_2 + O_{(a)} + [^*] \qquad \beta_1 \text{ peak}, \qquad [14]$$

$$N_{(a)} + N_{(a)} \rightarrow N_2 + 2[^*] \qquad \beta_2 \text{ peak}, \qquad [15]$$

where [*] denotes a free active site. The desorption temperature of the $\beta_2$ peak strongly depends on the surface coverage (17, 35–37), which is consistent with a second-order desorption process. In NO adsorption experiments, on increasing surface coverages, the $\beta_2$ peak fills up first and it moves toward lower temperatures. At higher coverages, most of the $N_2$ evolves as $\beta_1$, and $\beta_2$ is almost negligible (17, 36). Based on the above, the TPD peak observed at 440°C (Fig. 2C) may be associated with the $\beta_2$ peak discussed above. The absence of the $\beta_1$ peak is consistent with the absence of molecularly adsorbed NO, as shown in the corresponding FTIR spectrum (Fig. 1, h). The opposite is true in the case of the TPD spectrum of Fig. 4C, which is dominated by the $\beta_1$ peak.

### 4.3. *Effect of $W^{6+}$-Doping of $TiO_2$ on the Adsorptive Properties of Supported Rh*

Results obtained in previous studies in this laboratory revealed that chemisorptive behavior and kinetics of many reactions over noble metal crystallites can be significantly altered by doping of the $TiO_2$ carrier with small amounts (usually less than 0.5 at.%) of altervalent cations (28–30). These alterations are caused by charge transfer from the

**TABLE 2**

**Vibrational Frequencies of CO and NO Species Adsorbed over Rh Catalysts Supported on Undoped and $W^{6+}$-Doped $TiO_2$, at 250°C**

| Adsorbed species | Band frequency ($cm^{-1}$) | | Blue shift ($\Delta\nu$, $cm^{-1}$) |
|---|---|---|---|
| | $Rh/TiO_2$ | $Rh/TiO_2(W^{6+})$ | |
| $Rh–NO^+$ | 1910–1912 | 1920–1922 | 10 |
| $Rh(NO)_2$ | 1725 (asym) | 1750 | 25 |
| | 1830–1840 (sym) | 1870–1880 | 40 |
| $Rh–NO^-$ | 1770 | Not clearly distin- | |
| | 1660 | guishable | |
| Rh–CO | 2045 | 2050 | 5 |
| $Rh(CO)_2$ | 2094 (asym) | 2106 | 12 |

$TiO_2$ support to the metal atoms at the interface, originating from the fact that the work function of doped $TiO_2$ is lower than the work function of the metal. Comparison of the FTIR spectra obtained from Rh supported on undoped (Figs. 1 and 3) and $W^{6+}$-doped (Figs. 5 and 7) $TiO_2$ carriers shows that the vibrational bands related to adsorbed CO and NO species are shifted toward higher frequencies (blue shift) in the case of the doped catalysts (results are summarized in Table 2). Concerning adsorbed CO species, blue shifts of ca. 5 $cm^{-1}$ for the linear CO band and of ca. 12 $cm^{-1}$ for the *gem*-dicarbonyl band ($\nu_{asym}$) are observed when Rh is supported on the doped carrier. These values are in agreement with the corresponding ones of ca. 5–9 and 11 $cm^{-1}$, respectively, observed in a previous study where the effect of $W^{6+}$ concentration on the band positions of adsorbed CO species was investigated over similar catalysts (38).

The strengthening of the C–O bond, which is revealed by the blue shift over the doped catalysts, implies that the rhodium particles have an electronic configuration which does not favor the formation of Rh–CO bonds, as compared to the undoped catalysts. This result has been attributed to the intensified transfer of charge from the doped carrier to the Rh crystallites so that the supported Rh crystallites have a nearly saturated electronic configuration, which resembles that of silver or gold (38, 39, and Refs. therein).

The binding energy of CO to a metal surface occurs through the formation of a $\sigma$-bond by the overlap of an empty *d* orbital and a lone pair of the carbon atom of CO and the formation of a $\pi$-bond between a filled metal *d* orbital and an empty antibonding $\pi$-orbital ($\pi^*$) of CO. Then, if transfer of electrons from the doped carrier to the supported metal particles is assumed to partially fill the empty *d* orbitals of the surface atoms, the overlapping of empty Rh *d* orbitals and a lone pair of the C atom will be less effective in forming a Rh–CO bond. On the other hand, the ability of filled *d* orbitals to back donate electrons to the $2\pi^*$ orbitals of adsorbed CO will be enhanced due to greater availability of electrons. Consequently, the bonding between the CO molecule and the Rh site is weakened due to the unavailability of unoccupied states of Rh metal to form a $\sigma$-bond. Without a proper $\sigma$-bonding, back-donation of electrons from the *d* orbitals of the metal to the $2\pi^*$ orbital of CO (i.e., the $\pi$-bonding) cannot be efficiently conducted, even if the metal is enriched with electrons in the *d* orbitals (38, 39, and Refs. therein).

NO has an electronic structure very similar to that of CO and the corresponding molecular orbitals ($2\pi$ and $5\sigma$) involved in the formation of the metal–NO bond are the same. The only difference is that NO possesses an unpaired electron in the antibonding $2\pi$-orbital which, is the reason for a higher probability for dissociation of NO, compared to that of CO. The cationic species ($Rh–NO^+$) is produced by donation of an electron antibonding ($\pi^*_{2pz}$) of NO to the *d* orbital of the metal to strengthen the N–O bond, while the anionic one ($Rh–NO^-$) is produced by the transfer of a *d* electron of the metal to an antibonding $\pi^*_{2pz}$-orbital of NO to weaken the N–O bond. Due to these differences in the characteristics of bonding of the two species, $W^{6+}$-doping of $TiO_2$ is expected to affect, in a different manner, the positively and negatively charged species. The blue shift of $Rh–NO^+$ and $Rh(NO)_2$ bands may be explained in a way similar to that used for the Rh–CO and $Rh(CO)_2$ species discussed above. Doping results in weakening of the NO and CO bonds with Rh, which is also evidenced by the decreased amounts of desorbed species during the TPD experiments (Table 1).

Concerning the absorption bands of the two $Rh–NO^-$ species, although clearly present in the spectra obtained from the undoped catalyst at 1770 and 1660 $cm^{-1}$ (Figs. 1 and 3), they are not clearly observable in the corresponding spectra obtained from the doped catalyst (Figs. 5 and 7). This, of course, does not imply that these species do not participate in a dissociation step, but only indicates a decrease in the relative population of $Rh–NO^-$ on the doped catalysts. This can be explained by assuming that the N–O bond in the $Rh–NO^-$ species is further weakened by doping, resulting in higher rates of dissociation (Eq. [1]) and lower population of this species which, therefore, becomes undetectable under the present experimental conditions. This is evidenced by the transient-MS experiments obtained following the introduction of NO over the $H_2$-reduced (Fig. 6A) and CO-precovered (Fig. 8B) surfaces. Results show that significant amounts of dinitrogen are produced during the first few minutes, higher than the corresponding amount observed over the undoped catalysts (Table 1). This confirms that negatively charged species are present on the surface during the initial steps of adsorption, and indirectly proves the rapid dissociation of these species. Assuming that the rate-determining step is that of NO dissociation, the higher initial yield of $N_2$ observed over $Rh/TiO_2(W^{6+})$ as compared to that over the $Rh/TiO_2$ catalyst can then be

attributed to the larger value of the rate constant associated with this step.

## CONCLUSIONS

1. Nitrogen monoxide adsorbs molecularly on reduced $Rh/TiO_2$ catalysts at 250°C, giving rise to the formation of $Rh–NO^+$ and two different $Rh–NO^-$ species. The negatively charged species readily dissociate, when a neighboring reduced site is vacant, to form nitride and oxygen atoms. In the absence of an oxygen-atom scavenger, the catalyst surface becomes progressively oxidized due to the accumulation of oxygen atoms, thus favoring the formation of $Rh–NO^+$.

2. Under transient conditions of NO adsorption on $H_2$-reduced and CO-precovered surfaces, the population of $Rh–NO^+$ increases with the time of exposure at the expense of $Rh–NO^-$. The surface coverage of the latter species continuously decreases with time-on-stream as the reduced Rh sites become less available and drops to zero for oxidized surfaces. As soon as this happens, a dinitrosyl, $Rh(NO)_2$, species populates the surface.

3. The formation of dinitrogen in the gas phase occurs as long as $Rh–NO^-$ is present on the surface, while $N_2O$ production is related to the presence of the dinitrosyl species on the surface. However, the formation of both $N_2$ and $N_2O$ does not occur in the exclusive presence of $NO^+$ on the surface and in the absence of reduced Rh sites.

4. Displacement of NO(CO) by CO(NO) readily takes place at 250°C. There is no evidence for the formation of –NCO or Rh(NO)(CO) species under the experimental conditions employed.

5. Doping $TiO_2$ with $W^{6+}$ cations results in blue shifts in the stretching frequencies of N–O and C–O bonds contained in $Rh–NO^+$, $Rh(NO)_2$, Rh–CO, and $Rh(CO)_2$ species, indicating weaker bonding of the adsorbed molecules with the surface. This is also evidenced by the significantly lower amounts of accumulated species, desorbed during TPD. In contrast, the N–O bond of the $Rh–NO^-$ species is further weakened by doping, resulting in higher rates of dissociation and, concomitantly, in higher transient yields of $N_2$ in the gas phase, compared to that of the undoped catalyst.

## ACKNOWLEDGMENT

This work was partly funded by the Commission of the European Community, under Contract BRPR-CT97-0460.

## REFERENCES

1. Shelef, M., and Graham, G. W., *Catal. Rev.-Sci. Eng.* **36**, 433 (1994).
2. Armor, J. N., *Appl. Catal. B: Environ.* **1**, 221 (1992).
3. Taylor, K. C., *Catal. Rev.-Sci. Eng.* **35**, 457 (1993).
4. Iwamoto, M., Yahiro, H., Shunto, S., Yu-u, Y., and Mizuno, N., *Appl. Catal.* **69**, L15 (1991).
5. Kharas, K. C. C., Ribora, H. J., and Liu, D. J., *Appl. Catal. B: Environ.* **2**, 255 (1993).
6. Iwamoto, M., and Hamada, H., *Catal. Today* **10**, 57 (1991).
7. Oh, S.H., and Carpenter, J. E., *J. Catal.* **101**, 114 (1986).
8. Peden, C. H. F., Goodman, D. W., Blair, D. S., Berlowitz, P. J., Fisher, G. B., and Oh, S. H., *J. Phys. Chem.* **92**, 1563 (1988).
9. Yang, A. C., and Garland, C. W., *J. Phys. Chem.* **61**, 1504 (1957).
10. Rice, C. A., Worley, S. D., Curtis, C. W., Guin, J. A., and Tarrer, A. R., *J. Chem. Phys.* **74**, 6487 (1981).
11. Arai, H., and Tominaga, H., *J. Catal.* **43**, 131 (1976).
12. Hecker, W. C., and Bell, A. T., *J. Catal.* **84**, 200 (1983).
13. Solymosi, F., Bansagi, T., and Novak, E., *J. Catal.* **112**, 183 (1988).
14. Dictor, R., *J. Catal.* **109**, 89 (1988).
15. Hyde, E. A., Rudham, R., and Rochester, C. H., *J. Chem. Soc., Faraday Trans.* **80**, 531 (1984).
16. Anderson, J. A., Millar, G. J., and Rochester, C. H., *J. Chem. Soc. Faraday Trans.* **86**, 571 (1990).
17. Kaspar, J., de Leitenburg, C., Fornasiero, P., Trovarelli, A., and Graziani, M., *J. Catal.* **146**, 136 (1994).
18. Chuang, S. S. C., and Tan, C.-D., *J. Catal.* **173**, 95 (1998).
19. Srinivas, G., Chuang, S. S. C., and Debnath, S., *J. Catal.* **148**, 748 (1994).
20. Krishnamurthy, R., and Chuang, S. S. C., *J. Phys. Chem.* **99**, 16727 (1995).
21. Krishnamurthy, R., Chuang, S. S. C., and Balakos, M. W., *J. Catal.* **157**, 512 (1995).
22. Novak, E., Sprinceana, D., and Solymosi, F., *Appl. Catal. A* **149**, 89 (1997).
23. Liang, J., Wang, H. P., and Spicer, L. D., *J. Phys. Chem.* **89**, 5840 (1985).
24. Solymosi, F., and Sarkany, J., *Appl. Surf. Sci.* **3**, 68 (1979).
25. Chuang, S. S. C., and Tan, C.-D., *Catal. Today* **35**, 369 (1997).
26. Chafik, T., Efstathiou, A. M., and Verykios, X. E., *J. Phys. Chem. B* **101**, 7968 (1997).
27. Permana, H., Ng, K. Y. S., Peden, C. H. F., Schmieg, S. J., Lambert, D. K., and Belton, D. N., *J. Catal.* **164**, 194 (1996).
28. Ioannides, T., and Verykios, X. E., *Chem. Eng. Technol.* **18**, 25 (1995).
29. Ioannides, T., and Verykios, X. E., *J. Catal.* **161**, 560 (1996).
30. Zhang, Z., Kladi, A., and Verykios, X. E., *J. Phys. Chem.* **98**, 6804 (1994).
31. Papadakis, V. G., Pliangos, C. A., Yentekakis, I. V., Verykios, X. E., and Vayenas, C. G., *Catal. Today* **29**, 71 (1996).
32. Kondarides, D. I., Chafik, T., and Verykios, X. E., *J. Catal.*, in press.
33. Rethwisch, D. G., and Dumesic, J. A., *Langmuir* **2**, 73 (1986).
34. Casewit, C. J., and Rappe, A. K., *J. Catal.* **89**, 250 (1984).
35. Campbell, C. T., and White, J. M., *Appl. Surf. Sci.* **1**, 347 (1978).
36. Chin, A. A., and Bell, A. T., *J. Phys. Chem.* **87**, 3700 (1983).
37. Root, T. W., and Schmidt, D. L., *Surf. Sci.* **134**, 30 (1983).
38. Zhang, Z. L., Kladi, A., and Verykios, X. E., *J. Mol. Catal.* **89**, 229 (1994).
39. Akubuiro, E. C., and Verykios, X. E., *J. Catal.* **113**, 106 (1988).